CONF-8507117--3

93129

UCRL-
PREPRINT

LASER-DRIVEN INSTABILITIES IN LONG SCALELENGTH PLASMAS

W. L. Kruer

This paper was prepared for presentation at
the 29th Scottish Universities Summer School
in Physics to be held at St. Andrews, Scotland,
July 28-August 10, 1985

July 31, 1985

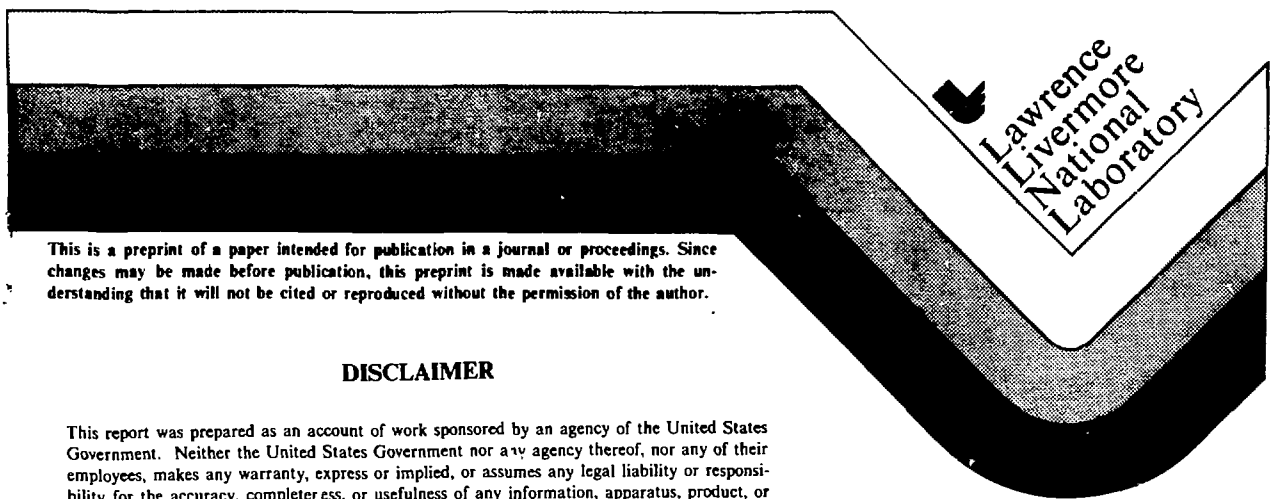

This is a preprint of a paper intended for publication in a journal or proceedings. Since changes may be made before publication, this preprint is made available with the understanding that it will not be cited or reproduced without the permission of the author.

DISCLAIMER

This report was prepared as an account of work sponsored by an agency of the United States Government. Neither the United States Government nor any agency thereof, nor any of their employees, makes any warranty, express or implied, or assumes any legal liability or responsibility for the accuracy, completeness, or usefulness of any information, apparatus, product, or process disclosed, or represents that its use would not infringe privately owned rights. Reference herein to any specific commercial product, process, or service by trade name, trademark, manufacturer, or otherwise does not necessarily constitute or imply its endorsement, recommendation, or favoring by the United States Government or any agency thereof. The views and opinions of authors expressed herein do not necessarily state or reflect those of the United States Government or any agency thereof.

DISTRIBUTION OF THIS DOCUMENT IS UNLIMITED

DISCLAIMER

This document was prepared as an account of work sponsored by an agency of the United States Government. Neither the United States Government nor the University of California nor any of their employees, makes any warranty, express or implied, or assumes any legal liability or responsibility for the accuracy, completeness, or usefulness of any information, apparatus, product, or process disclosed, or represents that its use would not infringe privately owned rights. Reference herein to any specific commercial product, process, or service by trade name, trademark, manufacturer, or otherwise, does not necessarily constitute or imply its endorsement, recommendation, or favoring by the United States Government or the University of California. The views and opinions of authors expressed herein do not necessarily state or reflect those of the United States Government thereof, and shall not be used for advertising or product endorsement purposes.

UCRL--93129

DE87 012908

LASER-DRIVEN INSTABILITIES IN LONG SCALELENGTH PLASMAS*

W. L. Kruer

Lawrence Livermore National Laboratory

ABSTRACT

In this update lecture we focus on laser-driven instabilities in long scalelength underdense plasmas. Particular attention is given to some recent experiments on Raman scattering of intense laser light. Many important features are in accord with theoretical expectations as discussed in lectures at previous summer schools. These features include a correlation of hot electron generation with Raman scattering, an increase in this scattering as the density scale length increases, and collisional suppression of the instability. Some challenging aspects of the growing data base as well as various deficiencies in the understanding are discussed. The role of the $2\omega_{pe}$, Brillouin, and filamentation instabilities is also briefly considered.

1. INTRODUCTION

Long scalelength plasmas are expected in laser fusion applications, since high gain capsules will be irradiated with long shaped pulses.[1] Effective pulse widths are of order 10 ns, leading to underdense plasma with density scale lengths of order 1 mm. As an illustrative example,[2] consider an Au disk

DISTRIBUTION OF THIS DOCUMENT IS UNLIMITED

MASTER

irradiated with a generic shaped reactor pulse of 0.26 μ light. Near the end of the pulse , the underdense plasma consists of two parts. The first is an ablatively steepened portion where inverse bremsstrahlung is efficiently depositing energy. In this high Z plasma, inverse bremsstrahlung begins to be quite efficient at densities of about a tenth of the critical density (n_{cr}), so the steepened portion of the profile extends to densities below 0.1 n_{cr}. The density scale length here is set by a competition between the deposition and the energy transport and is ∿ 400 μ for this example. At still lower densities, the plasma becomes isothermal with an electron temperature of ∿ 5 keV and a density scale length of ∿ 2 mm determined by the plasma expansion. The peak intensity is about 3×10^{15} W/cm^2 in this example, although lower peak intensities could be used. Note that the density scale length in the underdense plasma is > 2000 λ_0, where λ_0 is the free space wavelength of the light. Underdense plasmas with similar scale lengths are expected in low Z targets for direct drive applications.

As discussed in lectures at previous summer schools,[3] intense laser light can excite a variety of instabilities in long scalelength underdense plasmas. Most of these instabilities can be simply represented as the resonant decay of the incident light wave into two other waves. For example, if the unstable waves are a scattered light wave and an electron plasma wave (ion acoustic wave), we have the Raman (Brillouin) instability. If the unstable waves are both electron plasma waves, we have the two plasmon decay ($2\omega_{pe}$) instability. In addition, the incident light beam can filament and self-focus. These instabilities can lead to hot electron generation, scattering of the incident light, as well as significant nonuniformity in the irradiation. Hence, it is of considerable interest to understand the efficiency of these processes in long scalelength plasmas.

In these update lectures, we will consider some of the progress made in understanding and characterizing laser-driven instabilities in long scalelength plasmas. Our emphasis will be on Raman scattering, which to date has received the most attention because of

its role in generating hot electrons which preheat the fuel. Then the role of the $2\omega_{pe}$, Brillouin and filamentation instabilities will be briefly considered.

2.
RAMAN SCATTERING

Stimulated Raman scattering is a well-known process. The frequency and wave number matching conditions are

$$\omega_o = \omega_s + \omega_{ek}$$
$$\underline{k}_o = \underline{k}_s + \underline{k} \quad , \tag{2.1}$$

were ω_o (ω_s) and $\underline{k}_o$ ($\underline{k}_s$) are the frequency and wavenumber of the incident (scattered) light wave and ω_{ek} and $\underline{k}$ are the frequency and wavenumber of the electron plasma wave. This process leads to an instability since there's a feedback loop. Laser light with electric field E_L oscillating electrons in the presence of a small density fluctuation δn produces a transverse current ($\alpha\delta n\, \underline{E}_L$) which generates a small scattered light wave with electric field $\underline{E}_s$. This scattered light wave in turn beats with the incident field to reinforce the density fluctuation via the ponderomotive force ($\propto \underline{E}_L \cdot \underline{E}_S$). Hence the plasma wave and the scattered light wave grow at the expense of the incident light.

Since $\omega_s \geq \omega_{pe}$ (the electron plasma frequency), the process is limited to densities $< 1/4 n_{cr}$, where n_{cr} is the critical density. The maximum growth rate γ occurs for backscatter and is[3]

$$\gamma = \frac{k\, v_{os}}{4} \sqrt{\frac{\omega_{ek}}{\omega_s}} \quad , \tag{2.2}$$

where v_{os} is the oscillatory velocity of an electron in the field of the laser light. As an example, for .35 μ light with an intensity of 10^{15} W/cm^2, $\gamma \approx 2 \times 10^{-3}\, \omega_o$ at $n = 0.1\, n_{cr}$. The growth time is about .1 ps, quite short. Of

course, the wave coupling occurs even if it's not stimulated (i.e., if the instability is below its threshold). If the plasma wave is thermal level or enhanced by other processes, we simply have ordinary Raman scatter.

The threshold intensity for the Raman instability is determined by either damping of the unstable waves or by inhomogeneity in the plasma. A density gradient limits the region of resonant interaction. Propagation of the waves out of this interaction region represents a dissipation. As discussed in previous lectures, the gradient threshold intensities for backscatter (I_{TB}) and for sidescatter (I_{TS}) are

$$I_{TB} \simeq \frac{4 \times 10^{17}}{L_\mu \lambda_\mu} \frac{v_{gs}}{c} \frac{W}{cm^2}, \tag{2.3}$$

$$I_{TS} \simeq \frac{5 \times 10^{16}}{L_\mu^{4/3} \lambda_\mu^{2/3}} \frac{W}{cm^2} .$$

Here L_μ is the density scale length ($L^{-1} = 1/n\ \partial n/\partial x$) and $\lambda\mu$ the wavelength of the light in microns, and v_{gs} is the group velocity of the scattered light wave. The backscatter threshold corresponds to a convective amplification of $e^{2\pi}$, and the sidescatter threshold[4] is estimated for $n = 0.1\ n_{cr}$. Sidescatter has the lower gradient threshold, since the scattered light wave spends a longer time in the interaction region. For $n \sim 1/4\ n_{cr}$, $v_{gs}/c \sim (k_0 L)^{-1/3}$ and the thresholds for back and sidescatter become comparable.

In practice, gradients usually determine the threshold intensities. To illustrate the magnitudes, consider 0.35 μ laser light and a plasma with a scale length $L/\lambda_0 = 10^3$. Then $I_{TB} \sim 10^{15} W/cm^2$ and $I_{TS} \sim 3 \times 10^{13}\ W/cm^2$. The gradient thresholds can be significantly lower in a plasma with a density maximum.[5]

Threshold intensities are useful indicators but are, of course, only estimates since the calculations are ideal and the plasma

gradients are usually not well known. For example, threshold calculations typically assume a plane coherent light wave and a planar plasma slab. Experiments are characterized by a finite beam spot, intensity structure in the beam, and nonplanar plasma expansion. Hence, the scale length in the transverse direction can be comparable to that in the direction of expansion, an effect which can increase the threshold for sidescatter. In addition, temporal[6] and spatial incoherence[7] in the laser beam can raise the threshold. Significant affects are expected when $\Delta\omega > \gamma$ or when $(\Delta\theta)^2 > \gamma/\omega_0$. Here $\Delta\omega$ is the bandwidth, $(\Delta\theta)^2$ is the mean angular spread in the wave vectors of the pump, and γ is the growth rate of the instability.

In addition to the sizeable frequency shift of the scattered light, there are several other features of Raman scattering to be noted. First, sidescattering occurs preferentially out of the plane of polarization. The ponderomotive force due to the beat between the incident and scattered light waves then maximizes. In addition, we expect hot electron generation concomintant with Raman scattering. Part of the laser light energy is coupled into an electron plasma wave. When this plasma wave damps in a collisionless plasma, the faster, resonant particles are preferentially heated, resulting in suprathermal tails on the electron velocity distribution. As shown by the Manley-Rowe relations, $f_H = \omega_{ek}/\omega_s$ fs, where f_H (f_s) is the fraction of the laser energy absorbed into suprathermal electrons (scattered).

3.
SOME EXPERIMENTS ON RAMAN SCATTERING

With these general features in mind, let's now consider some recent experiments on Raman scattering in long scalelength plasmas. Many of the earlier observations[8-15] were already referred to in the lectures[3] at the previous summer school. These experiments included measurements[14] by Offenberger et al. of a Raman reflectivity of $\sim$.7% using 10.6 μ light as well as measurements[15] by Phillion et al. of a reflectivity of $\sim$10%

using 1.06 μ light. Since then many more experiments have been reported.[5,16-23]

A review is beyond the scope of these lectures. Instead, some recent experiments at the Lawrence Livermore National Laboratory on Raman scattering in long scalelength plasmas will be briefly discussed. These experiments serve to indicate some important trends as well as some areas in which the understanding is deficient. These observations include a correlation of hot electron generation with Raman scattering, an increase in this scattering as the density scale length increases, and collisional suppression of the instability. Poorly understood aspects of the data include the detailed frequency spectrum of the scattered light and the intensity thresholds for onset of the scattering. Indeed a low level signal is observed for low intensity irradiation, which might be simply ordinary Raman scattering from an enhanced level of plasma waves produced by another process.

Raman scattering is usually identified in experiments by the frequency (or wavelength) spectrum of the scattered light. Since the maximum allowed density is about $n_{cr}/4$, the frequency matching conditions give

$$\omega_0/2 < \omega_s < \omega_0 \quad , \tag{3.1}$$

$$\lambda_0 < \lambda_s < 2\lambda_0 \quad ,$$

where λ denotes the free space wavelength of the light. Figure 1 shows a typical measurement[22] of the scattered light signal as a function of wavelength in an experiment in which an Au disk is irradiated with 0.53 μ laser light with a peak intensity of a few times $10^{15} W/cm^2$. The signal is strongest at wavelengths which correspond to Raman scattering from densities $0.1 < n/n_{cr} < 0.2$. There is a small signal with wavelength near $2\lambda_0$, which may be Raman scattering near 1/4 n_{cr} or perhaps mode conversion of plasma waves generated by the $2\omega_{pe}$ instability. Note the "gap" in the signal which would correspond to Raman scattering for

densities $0.2 < n/n_{cr} < 0.24$. Note also the strong decrease in the signal at short wavelengths. Similar spectra have been observed in experiments at other laboratories.

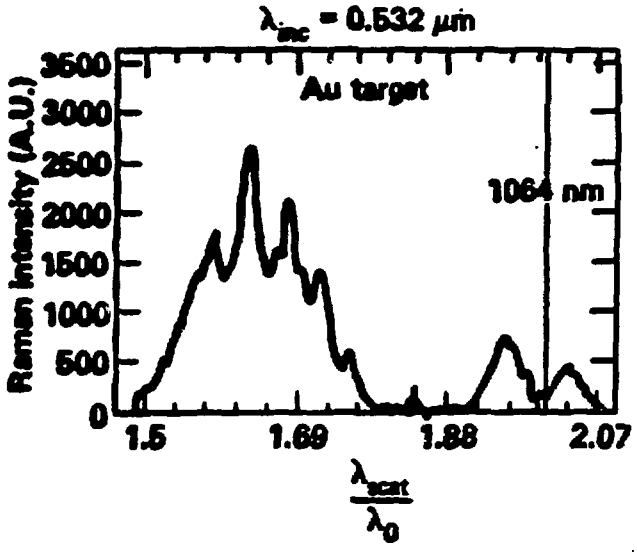

Fig. 1 The wavelength spectrum of light scattered by electron plasma waves in a Au disk[22] irradiated with a 1 ns pulse of .53μ light. The peak intensity was about $2 \times 10^{15} W/cm^2$.

The short wavelength cut-off is typically attributed to the suppression of the Raman instability at low plasma density due to strong Landau damping of the plasma wave. Indeed, the observed cut-off can be used to estimate[16] the electron temperature in the low density plasma. *If we estimate that strong Landau damping* onsets when $k \lambda_{De} \approx 0.3$, a cut-off at $\lambda_s \approx 1.5 \lambda_0$ indicates that $\theta_e \approx 3$ keV. Such estimates have been found to agree[22] with design code calculations and x-ray spectroscopy in thin CH foils. However, code calculations are typically somewhat higher (1.5-2x) than these estimates when thick disks are irradiated. This trend could provide a clue for modeling transport, since the thick disk targets are more sensitive to heat flow to high density.

The gap in the spectrum corresponding to Raman scattering from $0.2 < n/n_{cr} < 0.24$ presents a challenging puzzle. A variety of explanations have been offerred. Local steepening of the density profile near 1/4 n_{cr} by the 2 ω_{pe} instability might cause this effect. However, it's not clear that this instability is operative in the experiments at a sufficient level to cause the required steepening. A related possibility is the suppression of the Raman instability in this region by ion fluctuations concomintant with the nonlinear saturation of the 2 ω_{pe} and Brillouin instabilities. The gap corresponds to a regime in which the Raman instability generates plasma waves with relatively small $k \lambda_{De}$. Such long wavelength plasma waves may be particularly sensitive to collapse[25] accentuated by ion fluctuations. Finally, the gap may indicate that the Raman scattering is being seeded by an enhanced level of plasma waves excited by other processes. For example, Simon and Short[26] postulate that bursts of hot electrons due to the $2\omega_{pe}$ instability preferentially excite the plasma waves in the lower density region. Below the Raman instability threshold, we would then have ordinary Raman scattering from enhanced fluctuations. Above threshold, the instability grows from the enhanced levels. Here more calculations are needed to illustrate the plausible level of this enhancement.

Well above threshold, the Raman sidescattered light is observed to be preferentially out of the plane of polarization. Figure 2 shows the Raman scattered light (integrated over frequency) as a function of angle both in and out of the plane of polarization.[22] In the experiment a thin (2 μ) CH foil was irradiated with a 1 ns pulse of 0.53 μ light with a peak intensity of about 10^{15} W/cm^2. Note the strong asymmetry at significant angles between the measurements in and out of the plasma of polarization, as qualitatively expected.

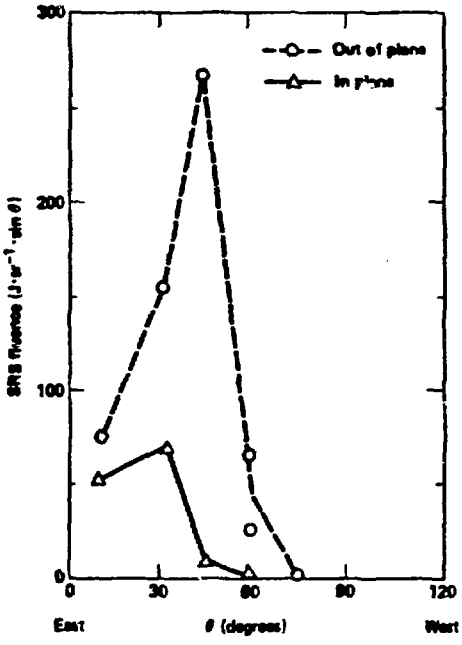

Fig. 2 An angular distribution of the light which was Raman-scattered from a CH foil[22] irradiated by a 1 ns pulse of .53μ light with a peak intensity of about $10^{15} W/cm^2$. The dashed (solid) line denotes measurements out of (in) the plane of polarization.

Raman scattering has also been observed to correlate with hot electron generation in experiments in which Au disk were irradiated with 1 ns pulses of 0.53 μ light. In these experiments,[21] the laser energy varied from .5 - 4 kJ and the nominal intensity from about 10^{14} - 2 X 10^{16} W/cm^2. Figure 3 shows the fraction of the laser energy deposited into hot electrons as inferred from the level of the hard x-rays versus the measured fraction of the laser energy which was in Raman scattered light. Note the impressive correlation. The solid line represents the expected correlation using the Manley-Rowe relations with the measured mean value of the frequency of the scattered light. Because of the error bars, it's quite possible that other processes such as the $2\omega_{pe}$ instability are also contributing to hot electron generation. A correlation between the Raman scattering and the hot electron generation (the high energy x-rays) has also been observed in time-resolved

measurements in experiments in which thin Au foils were irradiated with 1 ns pulses of .53 μ light.

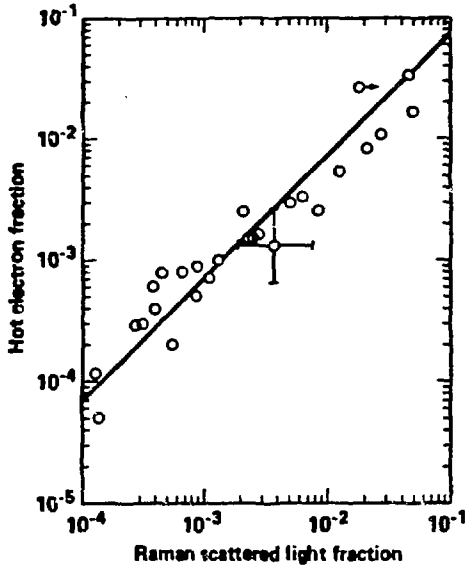

Fig. 3 The fraction of the laser energy absorbed into hot electrons versus the fraction in Raman-scattered light in Au disks irradiated by 1 ns pulses of .53μ light. See ref. 21.

The density scalelength near 0.1 n_{cr} in the thick disk experiments is estimated to be $L/\lambda_0 \sim 400$, varying somewhat as the focal spot was decreased to achieve the higher intensities. Hence the threshold for backscatter is about 3×10^{15} W/cm^2, and the threshold for sidescatter is about 10^{14} W/cm^2. Although there was significant scatter in the Raman signal as a function of intensity, the general trend was for the Raman reflectivity to increase from about 10^{-4} to several percent as the nominal intensity was increased from 10^{14} to 10^{16} W/cm^2. The reflectivity of 10^{-4} at intensities near 10^{14} W/cm^2 could be partially due to hot spots in the laser beam. Or this reflectivity could indicate an enhanced level of plasma waves generated in some other way. Another puzzling feature of the data is the growth of the Raman signal as a function of angle. Backscatter is

observed[22] to onset at about the same intensity as sidescatter does, rather than at the expected higher threshold intensity. This may indicate some difficulty in the backscatter theory or possibly microstructure in the plasma.

Finally, Raman scattering has been observed[23] both to increase when the density scalelength is further increased and to fall off dramatically near the collisional threshold of the instability. Underdense plasmas with larger density scale lengths were accessed by irradiating thin foil targets which expand to about 0.1 - 0.2 n_{cr} near the peak of the pulse. Some measurements of the fraction of the laser energy which is Raman scattered are shown in Fig. 4 for both CH and Au foils irradiated with either 0.53 μ or 0.26 μ laser light. In these experiments, the nominal intensity was > 10^{15} W/cm^2 and the pulse lengths were about 1 ns. The density scalelengths accessed are estimated to be L/λ_0 > 10^3. Note that an average Raman reflectivity of about 10% is found in the CH targets irradiated with 0.53 μ light (the peak reflectivity is even larger). Such a level is quite comparable to the predictions of computer simulations[27] and simple models.

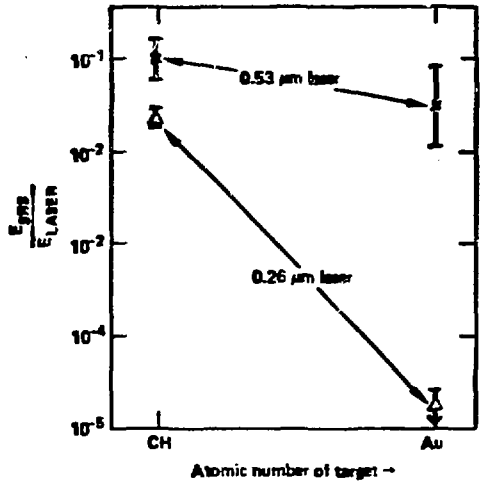

Fig. 4. Energy in Raman-scattered light from Ch and Au thin-foil targets. All cases have intensities > 10^{15} W/cm^2. The gold data point for 0.26 μm is an upper limit. See ref. 23.

The results in Fig. 4 also illustrate the effect of collisionality on Raman scattering. When CH foils are irradiated with 0.26 μ light, the plasma is denser and more collisional. The reflectivity dropped a factor of about three. Alternatively, the collisionality can be increased by using an Au foil. When Au foils were irradiated with 0.53 μ light, the Raman reflectivity was several times less than that observed with CH foils. Finally, for Au foils irradiated with 0.26 μ light, the plasma is estimated to be sufficiently collisional that the instability is stabilized. Indeed, the Raman reflectivity is observed[23] to drop to a very low level.

This brief discussion illustrates some of the progress in characterizing and controlling Raman scattering in long scalelength plasmas. Many significant trends well above threshold are in accord with expectations, but the detailed understanding is far from complete. Thin foil experiments are beginning to access plasmas with density scale lengths comparable to those expected in high gain targets. The results clearly indicate that sizeable Raman scattering can occur when the gradient and collisional thresholds are far exceeded. Of course, the plasma conditions in thin foils will differ in detail from those in overdense targets driven by long shaped pulses, and more work is needed to extrapolate to this regime. As emphasized by many experiments, more work is also needed to understand the frequency spectrum and angular distribution of the scattered light, the intensity and scalelength thresholds, and the noise level of the plasma waves. Detailed comparisons with theory are often made difficult by sizeable intensity structure in the laser beams, by poorly known plasma conditions, and by microstructure in the plasma due to other processes. This is a rich and no doubt a fruitful area for further research.

4.
THE $2\omega_{pe}$ INSTABILITY

Let's now briefly consider a related instability which can be operative in long scalelength plasmas. The $2\omega_{pe}$ instability

corresponds to decay of the laser light into two electron plasma waves. As apparent from frequency matching, the instability is limited to a narrow region near 1/4 n_{cr}. The maximum growth rate is equal to that of the Raman instability near 1/4 n_{cr}. The intensity threshold[28] I_T due to a density gradient is

$$I_T \sim \frac{4 \times 10^{15} \theta_{keV}}{\lambda_\mu L_\mu} \frac{W}{cm^2} , \qquad (4.1)$$

where θ_{keV} is the electron temperature in keV. This threshold is typically lower than that for Raman sidescatter, except in fairly long scale length plasmas. For example, for $\theta_{keV} \simeq 2$ the sidescatter threshold becomes lower when $L/\lambda_0 > 400$.

Since this instability generates high phase velocity electron plasma waves, hot electron production is a characteristic feature of the nonlinear state. The nonlinear state[28] is also characterized by local steepening of the density profile and by ion fluctuations nonlinearly generated by the plasma waves. The growth rate of the plasma waves, the density profile steepening, and the generation of ion waves have been measured in some detail in experiments[29] with 10.6 μ light. Although the results are qualitatively consistent with simulations, there are also discrepancies (for example, in the wavelengths[30] of the nonlinearly generated ion fluctuations). A useful signature of the instability is emission near $3/2\omega_0$, which arises from the coupling of the incident and reflected light with a plasma wave near 1/4 n_{cr}. Unfortunately the level of the instability is difficult to estimate from this signal since the emission only indirectly indicates the level of part of the spectrum of the plasma waves.

The $3/2\ \omega_0$ emission is frequently diagnosed in laser plasma experiments.[31-33] Some experiments[33] at the University of Rochester provide a recent example. In these experiments, CH spheres were irradiated with a 600-700 ps pulse of 0.35 μ light. The $3/2\ \omega_0$ emission was observed to onset at an intensity of about 2×10^{14} W/cm^2, the estimated threshold intensity of the

$2\omega_{pe}$ instability. The level of the emission increased with the intensity of irradiation but then saturated for an intensity of about 6 X 10^{14} W/cm^2 at a rather low level (10^{-9} of the incident energy). Hard x-rays indicating suprathermal electrons with a temperature of about 35 keV were observed to be correlated with the 3/2 ω_0 emission. The inferred fraction of the laser energy in these suprathermal electron also saturated at a low value of about 10^{-4} of the incident energy. The density scalelength in these experiments was estimated to be $L/\lambda_0 < 150$, decreasing as the target radius was reduced to achieve higher intensity. In experiments at Lawrence Livermore National Laboratory with longer scalelength plasmas and .53μ light, higher levels of $3/2\omega_0$ emission have been observed (up to about 10^{-4} of the incident energy). As already discussed, the hot electrons in these experiments correlated best with the Raman signal, but within the error bars there may also be some contribution from the $2\omega_{pe}$ instability.

Although difficult to quantify in experiments, the level of the $2\ \omega_{pe}$ instability seems puzzling. Simulations[28] without self-generated magnetic fields typically suggest an instability absorption > 5%, which is significantly greater than that generally attributed to this instability in experiments. Since the heat transport is not well understood, the profile steepening due to energy depositon near the critical density could extend down to densities < 1/4 n_{cr}. Alternatively, the rather low level might indicate additional choking of the instability by suprathermal tails if the fast electron transport is inhibited by magnetic fields[34]. Another possibilty is additional suppression due to ion fluctuations excited by the Brillouin instability. More work in this area is clearly needed.

5.
BRILLOUIN SCATTERING AND FILAMENTATION

Before concluding these update lectures, let's very briefly consider several instabilities which involve the growth of perturbations in ion density. It's well-known that stimulated Brillouin scattering

can occur in long scalelength plasmas. The feedback mechanism is similar to that for the Raman instability, except now the density fluctuation is associated with a low frequency ion acoustic wave. The growing ion fluctuations scatter the light, modifying the absorption and/or its location. In addition, these ion waves can indirectly affect other processes as mentioned in the previous sections.

For Brillouin scatter, gradients in the expansion velocity of the plasma typically limit the region of resonant interaction. The gradient threshold intensity I_{TB} for Brillouin backscatter then is

$$I_{TB} \sim 6 \times 10^{15} \frac{\theta_{keV}}{L_{\nabla v} \lambda_\mu} \frac{n_{cr}}{n} \frac{W}{cm^2} \quad , \tag{5.1}$$

where $L_{\nabla v}$ is the scalelength in microns for variation of the expansion velocity v_{exp}. In particular, $L_{\nabla v}^{-1} = 1/c_s \, \partial v_{exp}/\partial x$, where c_s is the sound speed. As is the case for the Raman instability, the threshold for sidescatter is lower by a factor of order $(\omega_0 L/c)^{1/3}$. As an example, for 0.35 μ light in a plasma with $n = 0.1\, n_{cr}$, $\theta_e = 2$ keV and $L_{\nabla v} = 10^3 \lambda_0$, $I_{TB} \sim 10^{15} W/cm^2$. The threshold for sidescatter is about a factor of 10 lower. A brief discussion of some of the nonlinear effects can be found in Ref 35.

Brillouin scattering remains a significant issue for long scalelength plasmas. Identification of the scattering by its frequency spectrum is often uncertain because of Doppler shifts in the expanding plasma. In some experiments[24] with large focal spots, much more light with frquency near ω_0 is observed to be scattered out of the plane of polarization than into the plane. In a number of experiments(36-39) with 1.06 μ and 10.6 μ light, a Brillouin reflectivity up to about 50% has been observed. However, in current experiments with shorter wavelength light, the reflectivety attributed to Brillouin scattering is typically < 20%. Important questions include the scaling of the reflectivity to longer scalelength plasmas and its angular distribution.

Filamentation is another potentially important process involving perturbations in ion density. In this instability, perturbations in the

intensity profile of an incident light beam grow in amplitude, causing the beam to break up into intense filaments. The feedback mechanism leading to instability is easy to understand. A local increase in the light intensity creates a depression in plasma density either directly via the ponderomotive force or indirectly via enhanced collisional absorption and subsequent plasma expansion. The density depression refracts the light wave into the lower density region, enhancing the intensity perturbations. The instability is termed either ponderomotive[42] or thermal[43-45] filamentation, depending on which mechanism generates the density depression. Self-focusing is the analogous process involving the entire beam.

Filamentation can significantly impact laser plasma coupling. Enhancements in intensity can introduce or modify other instabilities, change the location of the energy deposition, and possibly aggravate deleterious collective effects such as hot electron generation. Spatial structure in the irradiation pattern can enhance magnetic field generation, modify energy transport, and even degrade the symmetry and stability of implosions if the scalelength of the structure is sufficiently long. Filamentation can also complicate the interpretation of coupling and transport experiments, since the intensity in the underdense plasma is no longer a controlled variable and may be particularly sensitive to details of the beam profile.

A very simple treatment[46] suffices to illustrate the essential features of filamentation. Let's consider a plane light wave with intensity I propagating in the z direction in a plasma with uniform density n_o. We first calculate in the quasi-static limit the density perturbation, δn_e, induced by a perturbation in the intensity profile, where $I = I_o(1+\alpha\cos ky)$. In the case of ponderomotive filamentation,

$$n_e = n_o e^{-\frac{I}{2n_{cr}\theta_e c}}, \tag{5.2}$$

where n_e is the electron density, n_{cr} is the critical density, θ_e is the electron temperature, and c is the velocity of light. This equation is easily obtained by balancing the variation in electron pressure with the variation in the light wave pressure.

Hence Eq. 5.2 gives

$$\frac{\delta n_e}{n_o} = \frac{-\alpha\, I_o \cos ky}{2 n_{cr} \theta_e c} \quad , \tag{5.3}$$

where we have assumed that $I_o << 2n_{cr}\theta_e c$.

In the case of thermal filamentation, we simply balance the electron heat flow with the absorbed intensity:

$$\nabla\cdot(\kappa^T \nabla\theta_e) = -\kappa\, I \quad , \tag{5.4}$$

where κ^T is the classical electron thermal conductivity and κ is the spatial decay rate due to collisional absorption. The perturbation in intensity drives a perturbation in electron temperature which leads to a variation in electron density. In particular, we postulate

$$\begin{aligned} I &= I_o\,[1 + \alpha \cos ky], \\ \theta_e &= \theta_o\,[1 + \beta \cos ky], \\ n_e &= n_o\,[1 - \beta \cos ky], \end{aligned} \tag{5.5}$$

where we have invoked pressure balance transverse to the beam; i.e., the quasi-static limit. Only first order corrections are retained. With these variations in θ_e and n_e, we also have

$$\kappa^T = \kappa_o^T\,[1 + \tfrac{5}{2}\,\beta \cos ky], \tag{5.6}$$

$$\kappa = \kappa_o\,[1 - \tfrac{7}{2}\,\beta \cos ky], \tag{5.7}$$

where the subscript zero denotes the thermal conductivity and absorption coefficient evaluated at θ_o and n_o, the electron temperature and density in the absence of an intensity perturbation.

Substituting Equations (5.6) and (5.7) into Equation (5.4) gives to lowest order

$$\frac{\partial}{\partial z}\,\kappa_o^T\,\frac{\partial \theta_o}{\partial z} = -\kappa_o I, \tag{5.8}$$

and to next order

$$\beta = \frac{\kappa_0 I_0 \alpha}{6\kappa_0 I_0 + k^2 \kappa_0 T \theta_0} \quad . \tag{5.9}$$

Equation (5.8) determines θ_0, the electron temperature generated by the unmodulated beam. Equations (5.5) and (5.9) yield

$$\frac{\delta n_e}{n_0} \simeq \frac{-\kappa_0 I_0 \alpha \cos ky}{k^2 \kappa_0 T \theta_0} \quad . \tag{5.10}$$

Here we have assumed that $k^2 \kappa_0 T \theta_0 >> 6\kappa_0 I_0$, i.e., that the scalelength for temperature variation in the direction of propagation of the light wave is much longer than the wavelength of the intensity modulation in the transverse direction.

Comparing Equations (5.3) and (5.10) shows that

$$\left(\frac{\delta n_e}{n_0}\right)_t = \left(\frac{\delta n_e}{n_0}\right)_p \frac{2 n_{cr} \kappa_0 c}{k^2 \kappa_0 T} \quad , \tag{5.11}$$

where the subscripts t and p denote thermal and ponderomotive, respectively. For a high Z plasma,

$$\frac{2 n_{cr} \kappa_0 c}{k^2 \kappa_0 T} \simeq \frac{1}{7} \frac{\nu_{ei}^2}{k^2 v^2} \quad , \tag{5.12}$$

where ν_{ei} is the collision frequency appropriate to the high frequency resistivity and v_e is the electron thermal velocity. Hence thermal filamentation dominates for wavelengths $\lambda >> 10\lambda_{ei}$, where $\lambda_{ei} = v_e/\nu_{ei}$. To include the implicit Z dependence of the thermal conductivity, the right hand side of Eq. (5.12) is multiplied by a factor of about $\left(1 + \frac{3.3}{Z}\right)$.

The growth of these zero-frequency intensity modulations along with their self-consistent density fluctuations can easily be obtained from the standard dispersion relation[3] familiar from

discussions of Brillouin scatter:

$$\omega^2-k^2c_s^2 = \frac{k^2v_{os}^2\omega_{pi}^2}{4}\left[\frac{1}{D(\omega-\omega_o,\underline{k}-\underline{k}_o)} + \frac{1}{D(\omega+\omega_o,\underline{k}+\underline{k}_o)}\right] . \qquad (5.13)$$

Here $D = \omega^2-k^2c^2-\omega_{pe}^2$, c_s is the sound speed, ω_{pi} (ω_{pe}) is the ion (electron) plasma frequency, ω_o and $\underline{k}_o$ are the frequency and wavenumber of the incident light wave, and v_{os} is the oscillatory velocity of an electron in the incident light wave. The derivation assumes that there are no variations along the direction of the electric field vector of the light wave. To obtain ponderomotive filamentation, we look for zero frequency fluctuations with a wave vector orthogonal to the direction of propagation $\underline{k}_o$. In particular, we set $\omega = 0$ and take $\underline{k} = \underline{k}_r + i\underline{k}_i$, where $\underline{k}_r\cdot\underline{k}_o = 0$ and $\underline{k}_i$ is parallel to $\underline{k}_o$. Equation (5.13) then gives the dispersion relation

$$4k_i^2k_o^2 + k_r^4 - k_r^2\frac{\omega_{pe}^2}{c^2}\frac{v_{os}^2}{2v_e^2} = 0 . \qquad (5.14)$$

Growth maximizes ($\partial k_i/\partial k_r = 0$) when

$$k_r = \frac{1}{2}\left(\frac{v_{os}}{v_e}\right)\frac{\omega_{pe}}{c} ,$$

$$k_i = \frac{1}{8}\left(\frac{v_{os}}{v_e}\right)^2\frac{\omega_{pe}^2}{k_oc^2} , \qquad (5.15)$$

where we have also assumed that $Z\theta_e >> \theta_i$.

As shown in Eq. (5.11) the dispersion relation for thermal filamentation can be obtained from Eq. (5.13) by simply multiplying the intensity term by $\sim (7k_r^2\lambda_{ei}^2)^{-1}$. Then

$$4k_i^2k_o^2 + k_r^4 - \frac{v_{os}^2}{14v_e^2}\frac{\omega_{pe}^2}{c^2\lambda_{ei}^2} = 0 , \qquad (5.16)$$

where we have again assumed that $Z >> 1$. The growth now maximizes

for long wavelength:

$$k_r << \left(\frac{\omega_{pe}}{3.6c}\frac{v_{os}}{v_e}\frac{1}{\lambda_{ei}}\right)^{1/2} , \qquad (5.17)$$

$$k_i \approx \frac{\omega_{pe}}{7.5\, k_o c}\left(\frac{v_{os}}{v_e}\right)\frac{1}{\lambda_{ei}} .$$

We note that the maximum spatial gain coefficient for thermal filamentation exceeds that for ponderomotive filamentation when $\nu_{ei}/\omega_{pe} > v_{os}/c$. Hence the thermal mechanism is especially competitive in the denser, more collisional plasmas produced by short wavelength laser light.

To illustrate the numbers, let's consider some conditions typical of recent experiments[21] in which Au disks were irradiated with 1 ns pulses of .53 μ laser light. We take $I \approx 2\times10^{15}$ W/cm^2, $L_\mu \approx 250$ at $n_o/n_{cr} \approx .1$, $\theta_{kev} \approx 2$, and $Z = 50$. Then the minimum growth length ($\ell_g = 1/k_i$) for ponderomotive filamentation is about 60 μ for a filament with a wavelength of about 10 μ. There are several growth lengths for ponderomotive filamentation. The minimum growth length for thermal filamentation at $n = .1\, n_{cr}$ is about 300 μ for a filament with a wavelength much longer than about 20 μ. Of course, filamentation can be operative in longer scalelength plasmas at smaller intensities.

Unfortunately, filamentation in laser plasmas is perhaps the least understood and characterized of the processes we have discussed. An introductory discussion of possible nonlinear consequences is given in Ref. 46. Filamentation has been difficult to quantify in laser plasmas. Much of the evidence is rather indirect: inferences from structure[47-49] in x-ray pictures of the heated plasma or in images of the back-reflected light as well as inferences from the angular distribution[16] of half-harmonic light or from frequency shifts[40] in the reflected light. Recently, filamentary structures have been directly observed by using optical shadowgraphy,[50] by imaging the second harmonic

emission,[51] and by Thomson scattering[52] from electron plasma waves generated in the walls of the filament. Some experiments[50] with short wavelength light have also indicated that implosions are degraded when signs of filamentation are present. A better understanding of filamentation is clearly needed.

6.
SUMMARY

In summary, a variety of instabilities can play a role in the coupling of intense laser light with long scalelength plasmas. Improved understanding of these instabilities is important for the optimum use of large lasers in many applications. Experiments indeed show that at least some of the instabilities can be significant in laser fusion applications, although more work is needed to quantitatively extrapolate to targets irradiated with long shaped pulses. For example, some recent experiments on Raman scattering show many expected features, such as an increase in the scattering with density scalelength, a correlation with hot electron generation, and collisional suppression of the Raman instability in high Z plasmas irradiated with short wavelength light. As briefly discussed, there are also many aspects of the data which point to deficiencies in our understanding. Important topics for further study also include the competition of the instabilities and the role of filamentation in laser plasma experiments.

ACKNOWLEDGMENTS

I acknowledge valuable discussions with M. Campbell, P. Drake, K. Estabrook, R. Kauffman, B. Langdon, B. Lasinski, D. Phillion, R. Turner and E. Williams.

*Work performed under the auspices of the U. S. Department of Energy by the Lawrence Livermore National Laboratory under contract number W-7405-ENG-48.

References

1. J. Nuckolls, L. Wood, A. Thiessen, and G. Zimmerman, Nature 239, 139 (1972).
2. Barbara Lasinski (private communication, 1984).
3. W. L. Kruer, in Laser-Plasma Interactions (SUSSP Publications, Edinburgh, 1980), edited by R. A. Cairns and J. J. Sanderson, p. 388-430; also Laser-Plasma Interactions II (SUSSP Publications, Edinburgh, 1983), edited by R. A. Cairns, p. 185-204; and many references therein.
4. B. B. Afeyan and E. A. Williams, Lawrence Livermore National Laboratory UCRL-91595 (1984).
5. H. Figueroa, C. Joshi, H. Azechi, N. A. Ebrahim, and K. Estabrook, Phys. Fluids 27, 1887 (1984).
6. J. J. Thomson, Phys. Fluids 21, 2082 (1978); and references therein.
7. A. M. Rubenchik (private communication, 1983); A. B. Langdon, Lawrence Livermore National Laboratory, UCRL-50021-83 (1984), p. 3-35.
8. J. L. Bobin, M. Decroisette, B. Meyer and Y. Vittel, Phys. Rev. Letters 30, 594 (1973).
9. R. G. Watt, R. D. Brooks and Z. A. Pietrzyk, Phys. Rev. Letters 41, 170 (1978).
10. D. W. Phillion and D. L. Banner, Lawrence Livermore National Laboratory, UCRL-84854 (1980).
11. C. Joshi, T. Tajima, J. M. Dawson, H. A. Baldis and N. A. Ebrahim, Phys. Rev. Letters 47, 1285 (1981).
12. J. Elazar, W. Toner and E. R. Wooding, Plasma Phys. 23, 813 (1981).
13. K. Tanaka, L. M. Goldman, W. Seka, M. C. Richardson, J. M. Soures and E. A. Williams, Phys. Rev. Letters 48, 1179 (1982).
14. A. A. Offenberger, R. Fedosejevs, W. Tighe, and W. Rozmus, Phys. Rev. Letters 49, 371 (1982).
15. D. W. Phillion, E. M. Campbell, K. G. Estabrook, G. E. Phillips and F. Ze, Phys. Rev. Letters 49, 1405 (1982).
16. W. Seka, E. A. Williams, R. S. Craxton, L. M. Goldman, R. W. Short, and K. Tanaka, Phys. Fluids 27, 2181 (1984).
17. C. L. Shephard, J. A. Tarvin, R. L. Berger, Gar. E. Busch, R. R. Johnson, and R. J. Schroeder, KMSF U1562 (1985).

18. C. J. Walsh, D. M. Villeneuve, and H. A. Baldis, Phys. Rev. Letters 53, 1445 (1984).
19. R. G. Berger, R. D. Brooks, and Z. A. Pietrzyk, Phys. Fluids 26, 354 (1983).
20. R. E. Turner, D. W. Phillion, E. M. Campbell, and K. G. Estabrook, Phys. Fluids 26, 579 (1983).
21. R. P. Drake, R. E. Turner, B. F. Lasinski, K. G. Estabrook, E. M. Campbell, C. L. Wang, D. W. Phillion, E. A. Williams and W. L. Kruer; Phys. Rev. Letters 53, 1739 (1984).
22. R. P. Drake, Bull. Am. Phys. Soc. 29, 1229 (1984), E. M. Campbell et al., 14th Anomalous Absorption Conference, Charlottesville, Va. (1984), paper A4; R. P. Drake et al, ibid, paper A9; R. E. Turner et al, ibid, paper A10; D. W. Phillion et al, ibid, paper A11, R. L. Kaufmann et al, ibid, paper A12.
23. R. E. Turner, K. G. Estabrook, R. L. Kauffman, D. R. Bach, R. P. Drake, D. W. Phillion, B. F. Lasinski, E. M. Campbell, W. L. Kruer and E. A. Wiliams, Phys. Rev. Letters 54, 189 (1985).
24. E. M. Campbell, in Radiation in Plasmas (World Scientific Publishing Co., Singapore, 1984) Vol. I, edited by B. McNamara, P. 579-622.
25. D. Dubois, H. A. Rose, and D. R. Nicholson, Phys. Fluids 28, 202 (1985); and references therein.
26. A. Simon and R. L. Short, Phys. Rev. Letters 53, 1912 (1984).
27. K. Estabrook and W. L. Kruer, Phys. Rev. Letters 53, 465 (1984), and many references therein.
28. A. B. Langdon, B. F. Lasinski and W. L. Kruer, Phys. Rev. Letters 43, 133 (1979); B. F. Lasinski, A. B. Langdon, and W. L. Kruer, Lawrence Livermore National Laboratory, UCRL-50021-81 (1982), p. 3-30 and references therein.
29. H. A. Baldis and C. Walsh, Phys. Rev. Letters 47, 1658 (1981); also Phys. Fluids 26, 1364 (1981); and references therein.
30. D. M. Villeneuve and H. A. Baldis, paper D2, 15th Anomalous Absorption Conference, Banff, Canada, 1985.
31. R. E. Turner, D. W. Phillion, B. F. Lasinski and E. M. Campbell, Phys. Fluids 27, 511 (1983).
32. P. D. Carter, S. M. L. Sim, H. C. Barr and R. G. Evans, Phys. Rev. Letters 44, 1407 (1980)

33. R. L. Keck, R. L. McCrory, W. Seka and J. M. Soures, Phys. Rev. Letters 54, 1656 (1985).
34. J. M. Kindel, D. W. Forslund, W. B. Mori, C. Joshi, and J. M. Dawson, paper D3, 15th Anomalous Absorption Conference, Banff, Canada (1985).
35. W. L. Kruer and K. G. Estabrook, in Laser Interaction and Related Plasma Phenomena, Vol. 5, Edited by H. Schwarz, H. Hora, M. Lubin and B. Yaakobi (Plenum Press, New York, 1981), p. 783-800.
36. B. H. Ripin, F. C. Young, J. A. Stamper, C. M. Armstrong, R. Decoste, E. A. McLean and S. E. Bodner, Phys. Rev. Letters 39, 611 (1977).
37. D. W. Phillion, W. L. Kruer and V. C. Rupert, Phys. Rev. Letters 39, 1529 (1977).
38. A. Ng, L. Pitt, D. Salzmann and A. A. Offenberger, Phys. Rev. Letters 42, 307 (1979).
39. F. J. Mayer, G. E. Busch, C. M. Kinzer and K. G. Estabrook, Phys. Rev. Letters 44, 1498 (1980).
40. K. Tanaka, L. M. Goldman, W. Seka, R. W. Short and E. A. Williams, Phys. Fluids 27, 2960 (1984).
41. W. C. Mead, E. M. Campbell et al., Phys. Fluids 26, 2316 (1983).
42. P. K. Kaw, G. Schmidt and T. Wilcox, Phys. Fluids 16, 1522 (1973); B. I. Cohen and C. E. Max, Phys. Fluids 22, 1115 (1979); and references therein.
43. M. S. Sodha, A. K. Ghatak, and V. K. Tripathi, in Progress in Optics, Vol. 13, edited by E. Wolf (North Holland, Amsterdam, 1976); V. K. Tripath, and L. A. Pitale, J. Appl. Phys. 48, 3288 (1977); and references therein.
44. M. J. Herbst, J. A. Stamper, R. H. Lehmberg, et.al., Naval Research Laboratory Report 4983 (1981), and Proceedings of the 1981 Topical Conference on Symmetry Aspects of Inertial Fusion Implosions, Ed. S. Bodner, Naval Research Laboratory, Washington, D.C.
45. R. S. Craxton and R. L. McCrory, J. Appl. Phys. 56, 108 (1984); Kent Estabrook, W. L. Kruer and D. S. Bailey, Phys. Fluids 28, 19 (1985).
46. W. L. Kruer, Comments Plasma Phys. Controlled Fusion 9, 63 (1985).
47. R. A. Haas, M. J. Boyle, K. Manes and J. E. Swain, J. Applied Phys. 47, 1318 (1976); H. Shay et al., Phys. Fluids 21, 1634 (1978).

48. C. E. Max, et al., in Laser Interaction and Related Plasma Phenomena, Vol. 6, edited by H. Hora and G. Miley (Plenum, N.Y., 1984); W. C. Mead, et al., Phys. Fluids 27, 1301 (1984).
49. A. Ng, D. Saltzmann, and A. A. Offenberger, Phys. Rev. Letters 43, 1502 (1979).
50. O. Willi, in Laser Interaction and Related Plasma Phenomena, Vol. 6, edited by H. Hora and G. Miley (Plenum, NY, 1984).
51. J. Stamper, et al., Naval Research Laboratory Report 5173 (1984); M. J. Herbst, J. A. Stamper, R. R. Whitlock, R. H. Lehmberg, and B. H. Ripin, Phys. Rev. Letters 46, 328 (1981).
52. H. A. Baldis and P. B. Corkum, Phys. Rev. Letters 45, 1260 (1980).